



Extensional gravity-rheometry (EGR) for yield stress fluids

Anatole Geffrault, H. Bessaies-Bey, Nicolas Roussel, Philippe Coussot

► To cite this version:

Anatole Geffrault, H. Bessaies-Bey, Nicolas Roussel, Philippe Coussot. Extensional gravity-rheometry (EGR) for yield stress fluids. *Journal of Rheology*, 2021, 65 (5), pp.887-901. 10.1122/8.0000241 . hal-03857279

HAL Id: hal-03857279

<https://enpc.hal.science/hal-03857279>

Submitted on 17 Nov 2022

HAL is a multi-disciplinary open access archive for the deposit and dissemination of scientific research documents, whether they are published or not. The documents may come from teaching and research institutions in France or abroad, or from public or private research centers.

L'archive ouverte pluridisciplinaire **HAL**, est destinée au dépôt et à la diffusion de documents scientifiques de niveau recherche, publiés ou non, émanant des établissements d'enseignement et de recherche français ou étrangers, des laboratoires publics ou privés.

Extensional Gravity-Rheometry (EGR) for yield stress fluids

A. Geffrault^{1,2}, H. Bessaies-Bey², N. Roussel¹, P. Coussot¹

¹ Lab. Navier, Ecole des Ponts, Univ Gustave Eiffel, CNRS, 77420 Marne la Vallée, France

² MAST-CPDM, Univ Gustave Eiffel, 77420 Marne la Vallée, France

Abstract: In order to measure the extensional rheological properties of yield stress fluids, we developed a rheometrical approach based on the analysis of the deformations of a fluid extrudate flowing downwards and breaking in successive elongated drops due to gravity. Assuming the gradients of longitudinal velocity in radial planes are negligible, the local instantaneous strain rate is deduced from the variations of the filament diameter in each cross-section, while the normal stress is computed from the acceleration and weight of the material below this point. The observation of the filament profile in time allows to identify a solid region, in which the deformations tend to saturate, and a liquid region, in which the deformations continuously increase. A further analysis allows to distinguish the data for which pure elongational stress and strain rate components are effectively dominant, so that the elongational flow curve of the material over several decades of strain rate can be deduced. For two typical yield stress fluids (emulsion and clay suspension) with different internal structures, all the normal stress vs extensional rate data obtained under these different flow conditions fall along a single master curve for each material. This flow curve in elongation appears to be well represented by the standard 3D Herschel-Bulkley model under the condition that a slightly different power of the strain rate than in simple shear is used. For both material types, the elongational yield stress value found in this way is very close to the simple shear yield stress times the square root of three.

1. Introduction

The extrusion of YSF (yield stress fluids) is a very common industrial process, e.g. for foodstuffs, toothpastes, ceramic slips, plasters, mortars. In such processes, a gravity-induced free-surface flow may eventually shape the material. For 3D printing of YSF for medical applications [1], ink printing [2], construction materials [3-4], metals for applications in electronics [5], the extrusion then free surface flow of the filament followed by spreading and stoppage of the yield stress fluid determine the final shape of the object, and elongational flow can play a significant role in the different steps of these processes [6-8]. In this context a knowledge of the behavior of YSF in more complex flows than simple shear is required.

Here we focus on simple yield stress fluids, which in contrast with thixotropic yield stress fluids do not exhibit an apparent viscosity depending on the flow history [9-12]. In particular, these simple YSF exhibit identical static and dynamic yield stress, whatever the flow history. The constitutive equation of simple YSF was initially identified in simple shear [13-14], and the Herschel-Bulkley model [14] in simple shear is now classically shown to very well represent (steady state) flow curve data of various yield stress fluids [13]. The basic 3D expressions [15-18] of the constitutive equation of a YSF were built on the assumption of (i) an abrupt transition from the solid to the liquid regime, and (ii) a homogeneous behavior under any flow type, i.e. a constitutive equation with a yielding criterion and factors depending only on the second invariant of the strain rate tensor. The former assumption was then questioned, starting with Saramito [19], and various models were proposed in the last ten years, which are also associated with more sophisticated descriptions of the possible physical processes during this

transition [20-24]. The validity of the latter assumption (ii) has been discussed through various experimental approaches intending to measure the yield stress in elongation.

For a simple uniaxial elongation, the above “standard” Oldroyd 3D model [15-16] predicts that the yielding and slow flow should occur for a normal stress equal to $\xi\tau_c$ with $\xi = \sqrt{3}$. Here τ_c is the yield stress in simple shear, that we will simply call here the yield stress, while we will call the critical normal stress (i.e. σ_c) in a pure elongational flow, the elongation yield stress. As far as we know the experimental works in that field started with the study of the critical force of separation from either a drop elongation using a Capillary Breakup Elongational Rheometer (CaBER) [25], or a drop formation and fall from a die exit [26]. In each case a uniaxial elongational flow is assumed in the fluid around the region of breakage, and one measures the critical force at breakage, which is supposed to be balanced by capillary effect. In the first case [25], with emulsions, the critical normal stress was found to correspond to $\xi = 2.8$ whereas in the second case [26], with Carbopol gels, the expected expression (from above model) was found. Afterwards, a more complete study of the Laplace pressure in filaments [27] of various types of yield stress fluids led to the conclusion that the theoretical expression is found if the measurement is taken at a ratio of the filament life time to fluid relaxation time equal to 1. Moreover, experiments coupling CaBER with the application of an electrical field [28-29] allowed the estimation of the critical diameter for breakage of yield stress fluids, which proved to be in agreement with the standard prediction (i.e. $\xi = \sqrt{3}$). Another study looked at the viscous normal force all along the extension of a droplet between two plates and concluded to a larger critical normal stress $\xi = 3$ [30]. Finally an original approach with the same principle of plate separation but using smooth plates allowing an almost perfect wall slip (i.e. with wall slip yield stress close to zero), and thus a priori a homogenous elongational flow in the whole sample, concluded that the ratio of the elongation yield stress to the shear yield stress is larger (i.e. $\xi = 1.5\sqrt{3}$) than expected from the standard theory [31]. The discrepancy between theory and experiments concerning this problem was suggested to be due to the fact that the effective constitutive equation should also include a term depending on the third invariant of the stress tensor [25], or that significant shear flow components are not taken into account [30]. Alternatively, it was suggested that the pinch-off behavior of yield stress fluids presents nonuniversal trends that should be described with the help of nonlocal rheological models [32]. The recent approach of Varchanis et al [33], based on the Optimized Cross-Slot Flow Geometry, in some way went farther as an elongational flow could be maintained, so that the validity of the constitutive equation in the liquid regime could be tested. Further work clearly appears necessary in that field.

Actually, a more straightforward, “rheometrical”, i.e. without preliminary assumption on the constitutive assumption, characterization of the YSF behavior under extensional flow conditions would be useful, as we have for polymers. For other non-Newtonian fluids such as viscoelastic [34-36] or pseudoplastic fluids [6], the usual technique consists to stretch a liquid bridge between two plates moving away from each other [37-41]. However, this technique is problematic with YSF with a significant yield stress, as, during extension, the bridge readily breaks in two cones [42] which then keep their shape under gravity. Under these conditions, the normal stress rapidly increases in the pinch-off region and a significant shear component may develop (see the simulations by Moschopoulos et al [43]). Thus, for YSF the flow is not homogeneous in some significant central region as it can be with simpler fluids, and the flow characteristics more rapidly vary than for simpler fluids, so that it is more difficult to make measurements.

A dripping experiment might be more favorable, as the fluid is now not constrained by its contact with some lower boundary, so that it is freer to elongate. In general dripping is more difficult to control: the

evolution of the shape of the filament, possibly as one or several drops, results from the coupling between surface tension effects, flow discharge and the detailed rheological behavior of the material. This is a very complex process [44], even with simple liquids [45]. As explained in Sharma et al [46] with regards to their so-called ROJER technique, i.e. an analysis of dripping under gravity, in that case “the rheometry technique is based on the understanding of the nonlinear fluid dynamics underlying the jetting process”.

As shown by Gaulard and Coussot [47] the dripping of a yield stress fluid from a conduit has interesting specificities: it evolves in successive droplets of shape and size which may be related to the rheological behavior of the material. The detailed characteristics of these droplets were studied in the context of filament flow and breakage under gravity [48] and the flow between two plates moving away [43] for yield stress fluids of constitutive equation following the standard model. These works provided much information concerning flow regimes and flow characteristics certainly applicable to yield stress fluids in general.

In the present paper, we evaluate the possibility to directly determine, through experimental measurements, the rheological properties of yield stress fluids in extensional flows without preliminary assumption on the constitutive equation (except the existence of a solid-liquid transition at an indeterminate stress value). In that aim we propose to analyze the fluid flow during dripping after extrusion through a die. A great advantage of this geometry is that the normal stress at some point directly depends on the weight of material situated below this point. As a consequence, the stress increases progressively from zero along the sample axis, and a simple measure of the sample shape provides both the value of the local stress and the current local deformation.

We first present a theoretical analysis of the problem, which aims at extracting the means to determine experimentally the stress vs strain rate relationship (see Section 2). Then we test this approach through a few experiments with two material types. In Section 3 we present the materials and procedures, and in Section 4 we present and discuss the results.

2. Theoretical aspects: extensional rheometry for YSF

2.1 General flow conditions

We consider the downward flow of a YSF through a vertical die. As for standard rheometry which does not a priori assume some specific rheological behavior of the fluid under study, for the theoretical developments below, the only assumption we make on the YSF material behavior is that, under given boundary conditions, it can flow steadily only if some characteristic stress of this flow is larger than a critical value (i.e. a yield stress; e.g. τ_c in simple shear). The ground surface below the die is situated at a sufficiently large distance to preclude the contact of the extrudate with the ground before filament breakage. Thus, we expect the formation of more or less long drops successively falling to the ground. A typical example of such a process is shown in Figure 1. Note that successive longer drops are obtained when increasing the extrusion rate [47]. This means that the sufficient distance to preclude the contact of the extrudate with the ground before filament breakage may need to be adjusted as a function of the extrusion rate.

Let us focus on the flow characteristics just after a breakage of the filament, leading to the formation and fall of a drop. The fluid situated above this drop forms a filament that is still connected to the die. As a first approximate, the normal stress at some point in this fluid is equal to the weight of material situated below this point divided by the area of the filament cross-section at this point. Thus, the normal stress increases upwards from the filament bottom. Since we are dealing with a YSF, we expect that, along some distance, the stress is below some yield stress of the material so that the filament just undergoes finite deformations, whereas, beyond this distance (from the filament bottom), the

fluid starts flowing in its liquid regime. This flow ultimately leads to the breakage of the filament at some point.

Actually, the transition cannot simply be deduced from the values of the initial filament diameter and some elongational yield stress (i.e. σ_c). Indeed, according to the above estimation of the normal stress (weight to section area), in a given fluid point the normal stress increases when the filament deforms since the section diameter decreases. This is in particular true for the filament parts in the solid regime. This implies that the exact position of the transition along the filament depends on the deformations undergone in the solid regime.

Furthermore, the flow at larger distances from the filament bottom starts later (when the material appears at the die exit) but is faster since the stress is larger. This implies that the point of breakage depends on the detailed fluid behavior and the extrusion rate.

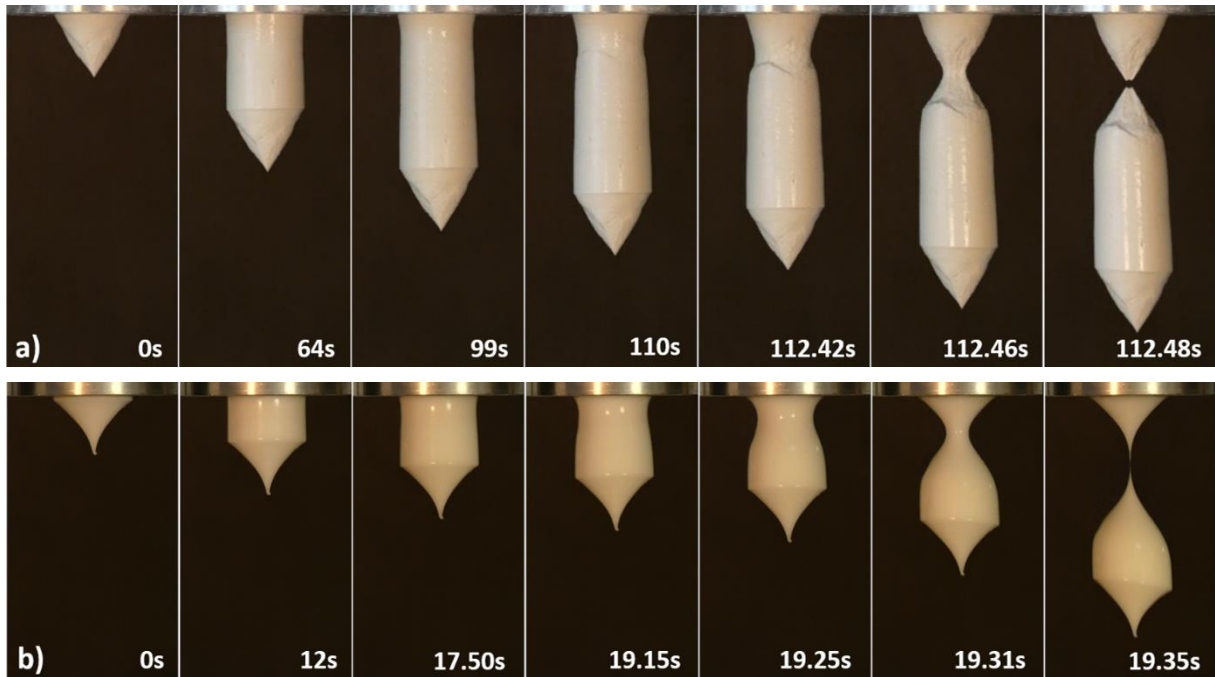


Figure 1. Successive aspects of the filament (diameter 2 cm) during extrusion from the initial time (breakage of the previous drop) to the next breakage for: (a) the kaolin suspension at 0.36 mm s^{-1} and (b) the emulsion at 0.9 mm s^{-1} .

It must also be noticed that, since, before breakage, the stress was larger than the yield stress in some region above the breakage point, the fluid has been significantly deformed too (see Figure 1). This region will correspond to the bottom of the next drop, i.e. the region around point O in Figure 2. This implies that the bottom of each drop is widely deformed along some distance. Above this distance we then have a slightly deformed region corresponding to the exit of the filament from the die after the previous drop breakage (see Figure 2).

Finally, this type of flow is particularly interesting as:

- 1) The stress results from gravity and is therefore controlled;
- 2) The observation of the filament size evolution directly provides information on the deformation history.

The above suggests that some proper approximations and analysis could allow for the extracting of some important information concerning the constitutive equation of the material.

Note that we aim here at describing the problem at best in the absence of any *a priori* knowledge about the constitutive equation of the material, except the fact that it exhibits a “solid-liquid transition” for a critical stress. Let us nevertheless recall that we further assume that the fluid is a non-thixotropic one. As a corollary of this assumption, there is no impact of the flow history on the fluid behavior and thus its rheological properties are not affected by the flow in the extruder, i.e. as soon as it emerges from the extruder it has recovered its original properties corresponding to a material at rest.

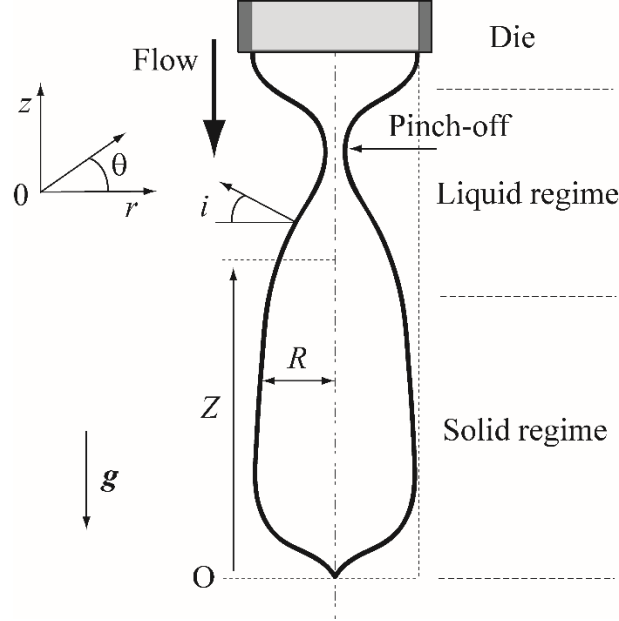


Figure 2. Scheme of the shape of a filament of yield stress fluid after the exit from the die. Depending on the normal stress value induced by gravity acting on the volume below the induced deformations lead the material to be in its solid or in its liquid regime.

2.2 Flow characteristics

Let us consider the gravity flow resulting from the fluid extrusion shown in Fig. 2, and describe it in a cylindrical reference frame r, θ, z . We consider the situation, for which the solid region has been deformed to its final state (i.e. associated with finite deformations (see Section 2.1)), and we focus on the flow characteristics in the liquid region. In the absence of any flow instability, the velocity components in the cylindrical frame (i.e. v_r, v_θ, v_z) are independent of the angle θ and there is no rotation, so that $v_\theta = 0$. Under these conditions, the mass conservation writes:

$$\frac{1}{r} \frac{\partial(r v_r)}{\partial r} + \frac{\partial v_z}{\partial z} = 0 \quad (1)$$

As the filament cannot be considered as slender (see Figure 1) we cannot make this usual assumption which readily leads to natural simplifications in the flow field and stress tensor. Nevertheless we will make a fundamental assumption concerning the flow field: we assume that beyond some short distance from the die exit the longitudinal velocity does not depend on the distance from the central axis, i.e. $v_z = f(z, t)$. This simplification derives naturally from the slender filament assumption for a flow not submitted to external shear stresses, but is less obvious when the filament radius rapidly varies, which is our case here. However, we can remark it is consistent with our specific boundary conditions: in the solid regions, which lie at the lower boundary of the liquid region, the velocity is uniform (plug), so it is effectively independent of r ; in the pinch-off region the flow, in a reference

frame moving with this point, is approximately anti-symmetrical with regards to a horizontal plane passing through this point; this implies that the longitudinal velocity is zero at any point of the pinch-off cross-section in a frame moving with this region, and thus is uniform in the laboratory frame.

It follows from this assumption that the material in a thin horizontal layer progressively undergoes an elongational flow under a constant total vertical volume force resulting from the gravity acting on the material below this layer. However, the corresponding normal stress increases in time if the section area decreases. Moreover, the flow is more complex than a pure elongational flow as each horizontal layer is elongated at a different rate (the vertical force acting on it being different), which induces some shear in the radial direction. We will discuss further the impact of such effects on the flow characteristics. In any event, we will now follow the fluid motion in one such layer, which means that our referential frame is attached to it.

From equation (1) it follows that $v_r = -\frac{r}{2}\dot{\epsilon}$, in which $\dot{\epsilon} = \frac{\partial f(z,t)}{\partial z}$ is the local, instantaneous, extensional rate. Writing this equation for $r = R$, the external radius of the layer under consideration, for which $v_r = -dR/dt$, we deduce:

$$\dot{\epsilon} = \frac{2}{R} \frac{dR}{dt} \quad (2)$$

In practice, R is determined as a function of time and of some distance from some fixed reference point. This explains that, in (2), we use a material derivative as it is necessary to follow the size variations of the layer during its vertical motion.

As already mentioned, the above flow is not a pure elongational flow since $\dot{\epsilon}$ depends on z . The strain rate tensor finally writes:

$$\mathbf{D} = \begin{bmatrix} -\dot{\epsilon}/2 & 0 & -(r/4)(\partial\dot{\epsilon}/\partial z) \\ 0 & -\dot{\epsilon}/2 & 0 \\ -(r/4)(\partial\dot{\epsilon}/\partial z) & 0 & \dot{\epsilon} \end{bmatrix} \quad (3)$$

We now focus on the stress tensor Σ , of components $\sigma_{rr}, \sigma_{r\theta}, \dots$. In the absence of flow instability, there is no effect tending to induce a rotation of the fluid around its axis, so that the stress components $\sigma_{\theta z}$ and $\sigma_{r\theta}$ are equal to zero, and the other components of the stress tensor are independent of θ . In consistency with the above assumption for $f(z)$, we assume that σ_{zz} is constant in a section, i.e. it is independent of r for a given value of z and at a given time. We assume this is the same for the other diagonal components of the stress tensor, i.e. $\sigma_{\theta\theta}$ and σ_{rr} . At last, in this theoretical approach, we will neglect surface tension effects.

The momentum equation in the z -direction gives:

$$\frac{1}{r} \frac{\partial(r\sigma_{rz})}{\partial r} + \frac{\partial\sigma_{zz}}{\partial z} - \rho g = \rho a \quad (4)$$

in which $a = a(z,t) = dv_z/dt$ is the acceleration of the fluid element. This equation may be multiplied by r and integrated between 0 and R , to get:

$$2 \frac{\sigma_{rz}(R)}{R} + \frac{\partial\sigma_{zz}}{\partial z} - \rho g = \rho a \quad (5)$$

Besides, we have the boundary condition $\Sigma \cdot \mathbf{n} = 0$ along the external surface of the sample, where we can write $\mathbf{n} = \mathbf{e}_r \cos i + \mathbf{e}_z \sin i$, in which i is the angle between the normal to the surface and the horizontal. We deduce:

$$\sigma_{rr}(R)\cos i + \sigma_{rz}(R)\sin i = 0 \text{ and } \sigma_{rz}(R)\cos i + \sigma_{zz}(R)\sin i = 0 \quad (6)$$

The angle i is defined through $\tan i = -\partial R/\partial z$, so that $\sigma_{rz}(R) = \sigma_{zz} \partial R/\partial z$. Under these conditions, Eq. (5) may be rewritten as:

$$\frac{\partial}{\partial z}(R^2 \sigma_{zz}) = \rho(g + a)R^2 \quad (7)$$

In practice, we can measure the shape of the drop in time, from direct observations. This typically gives the function $R(z, t)$ in the laboratory frame. Nevertheless, for the description it is more practical to describe the filament geometry in a frame moving with the drop tip, in order to focus on the filament deformation in time. Thus, we move from an Eulerian to a Lagrangian approach and describe the height along the filament in this moving frame, with the variable Z . The origin of this frame, i.e. the point O for which $Z = 0$, is taken at the drop tip.

The integration of equation (7) between 0 and Z then gives:

$$\sigma_{zz} = \frac{mg + q}{\pi R^2(Z, t)} \quad (8)$$

In which $m = \int_0^Z \rho \pi R(z, t)^2 dz$ is the mass of material below the height Z , and $q = \int_0^Z \rho \pi R(z, t)^2 a(z, t) dz$.

Note that, in contrast with detailed analyses [43, 48], previous works such as [26, 47] aiming at directly determining the elongational yield stress, generally neglected inertia effects, so that the normal stress is assumed to be given by (8) without the acceleration term q . We will show later (see experimental results) that these effects play a critical role in the last times of the flow because the drop strongly accelerates just before its separation. This term is therefore needed to get more relevant data from image analysis.

In addition, from (6) we find

$$\sigma_{rr}(R) = (\tan^2 i) \sigma_{zz}(R) \quad (10)$$

from which we deduce that the component σ_{rr} of the stress tensor is negligible as compared to σ_{zz} if $\tan i$ is sufficiently small.

At last, we can deduce the expression for σ_{rz} from equation (4) after integration between 0 and r using the independence of various terms with regards to r , and using the expression for this stress for $r = R$ (equation 6). We finally get:

$$\sigma_{rz} = \left(\rho(g + a) - \frac{\partial \sigma_{zz}}{\partial z} \right) \frac{r}{2} = -\frac{r}{R} \sigma_{zz} \tan i \quad (11)$$

2.3 Elongation rheometry from drop shape observation

As soon as $R(Z, t)$ has been determined, the normal stress $\sigma_{zz}(Z, t)$ may be deduced from (8) by computing m and q by integration over the filament. Then $\sigma_{rz}(Z, t)$ follows from (11), in which we can introduce $\tan i = -\partial R/\partial Z$.

In parallel, the elongational rate $\dot{\varepsilon}$ can be computed as a function of the experimental data. In the material derivative of (1), we now have to take into account that the position of a given fluid layer situated in Z at some time varies with time. It follows that

$$\frac{dR}{dt} = \frac{\partial R}{\partial t} + \frac{\partial Z}{\partial t} \frac{\partial R}{\partial Z} \quad (12)$$

All the terms in the right hand-side may be directly computed from the $R(Z,t)$ measurements. In order to get $\partial Z/\partial t$, we can take advantage of the mass conservation, which tells us that, if we follow a given fluid layer, $\int_0^Z \rho \pi R^2 d\xi$ is constant. It follows that $\frac{\partial Z}{\partial t} = -\frac{2}{R^2} \int_0^Z R \frac{\partial R}{\partial t} dz$, so that finally

$$\dot{\epsilon}(Z,t) = \frac{1}{R} \frac{\partial R}{\partial t} - \frac{2}{R^3} \frac{\partial R}{\partial Z} \int_0^Z R \frac{\partial R}{\partial t} dz \quad (13)$$

Also, the acceleration corresponds to $a = a(z,t) = dv_z/dt = \partial(v(Z))/\partial t$, where $v(Z) = v(O) + \partial Z/\partial t$. Thus a may be expressed as $a = -a_0(t) + b(z,t)$, in which $a_0 = \partial v(O)/\partial t > 0$ is the acceleration amplitude of the drop bottom with regards to the laboratory referential and $b = \partial^2 Z/\partial t^2 > 0$, an opposite acceleration due to the drop deformation. The expression for q can now be written as the sum of a term associated with a_0 and a term associated with b (integral between 0 and Z). In general, inertia effects become significant in the last time of the flow before breakage. In that case, $b = 0$ in the solid region and is very low in most of the liquid region except at the approach of the pinch-off region where most of the flow is localized. This implies that, in the integral (equation (9)) associated with the component of q resulting from b , the integrated function is equal to zero or very small over most of the range of integration. Thus this component is negligible and we simply have $q = -ma_0$.

Thus, by measuring the shape of the drop in time, i.e. $R(Z,t)$, we can deduce the strain rate tensor and the stress tensor, and thus establish the relationship between the two, i.e. the constitutive equation under such flow conditions close to simple elongation.

2.4 Limitations

Elongational vs shear components

In view of our objective to have a technique for measuring the elongational properties of the fluid we are seeking for flow conditions from which we can directly extract a relationship between the normal stress and the elongational strain rate. However, the flow under study is in general not a purely elongational one, i.e. in which we could readily neglect the stress components other than σ_{zz} and the components of the strain rate tensor other than the diagonal ones. For the stress tensor, the discrepancy from these ideal conditions appears to mainly depend on the value of $\tan i$, which determines the importance of the stress components other than σ_{zz} with regards to σ_{zz} for $r = R$ (cf. equations (10) and (11)). According to equation (11) a value smaller than 0.1 for $\tan i$ ensures that the σ_{rz} will be smaller than 10% of σ_{zz} , and would thus appear sufficient for an evaluation of the constitutive equation at first order, as usually assumed in rheometry. Remark that in that case our assumption of negligible σ_{rr} value would also be clearly validated (according to (10)), and $\sigma_{\theta\theta}$, which can be expected to play a role similar to σ_{rr} with regards to σ_{zz} , would also be negligible, but the latter assumption is not central in our work.

For the strain rate tensor, the discrepancy from these ideal conditions depends on the value of $\beta = (R/4\dot{\epsilon})(\partial\dot{\epsilon}/\partial z)$ which determines the relative importance of the shear and the elongation components in the velocity field. A sufficiently low value for beta should ensure the negligibility of the non-diagonal components of the strain rate tensor. As a consequence, we could a priori consider again

that a value for β smaller than 0.1 should ensure the negligibility of the shear component for an evaluation of the behavior at first order. However, it is worth noting that the exact impact of the shear rate component in the normal stress vs strain rate relationship depends on the form of the constitutive equation of the material. For example, for the standard Oldroyd 3D expression of the Herschel-Bulkley model (see Section 4.2), the shear rate just appears in the relation between σ_{zz} and $\dot{\epsilon}$ through the second invariant of the strain rate tensor, so that a value of β smaller than 0.4 is sufficient to ensure that it affects by less than 10% this constitutive equation in elongational flow (see Appendix 1).

Surface tension effects

Surface tension effects are obviously expected to start playing a role if viscous effects are sufficiently low. It seems difficult to establish general criterion for surface tension effects being negligible for this flow type. Indeed, a complete approach should take into account the gradient of the Laplace pressure induced by the filament curvature, and its evolution in time and along the drop axis, as a result of the complex curvature evolution. A detailed study of the impact of surface tension on the filament shape and breakage characteristics was carried out in the case of a fluid following a Herschel-Bulkley model [48]. Here we just propose a basic approach which compares the order of magnitude of viscous effects under slow flow (i.e. when the stress is in the order of the yield stress) conditions and surface tension effects. In this aim we compare the work associated with the main stress (i.e. the normal stress) during some elementary strain in a layer of initial thickness h and radius R , i.e. $-(\pi R^2 h) 2\sigma_{zz} dR/R$, to the surface energy variation resulting from this deformation, i.e. $\gamma d(2\pi R h) = -2\pi h dR$ (where γ is the surface tension of the fluid). We deduce that surface tension effects will be negligible if $\sigma_{zz} R \gg \gamma$. In the liquid region, the radius is smaller than R_0 the initial radius, but the normal stress approximately increases with $1/R^2$ (assuming a constant weight), so that $\sigma_{zz} R$ increases when R decreases. It follows that it is sufficient to have $\sigma_c R_0 \gg \gamma$ for surface tension effects to be negligible. Note that, according to previous studies [30], it can be considered that the surface tension of such materials is close to that of their interstitial liquid, which is often water, so in that case we have $\gamma \approx 0.07 \text{ N m}^{-1}$. The above result is similar to that obtained from a direct comparison of the characteristic stress in the material for sufficiently slow flows, i.e. σ_c , and the characteristic capillary stress, i.e. γ/R_0 , associated with the initial curvature of the filament.

3. Materials and methods

3.1 Materials

We chose to use two model yield stress fluids of different structure types, which a priori do not exhibit thixotropic properties and whose yield stresses are relatively large. We prepared a concentrated direct emulsion from dodecane oil (88% of the total volume) and an aqueous solution containing 3% of TTAB, an ionic surfactant. The emulsion was prepared by slowly pouring the oil into the water solution while mixing with a Silverson mixer at 500 rpm. Once the oil was poured entirely, the rotation speed of the mixer was increased by steps, up to 6000 rpm, to finally disperse the oil into droplets of diameter $\approx 2\mu\text{m}$. Its density is 800 kg m^{-3} . This material type is essentially a simple (non-thixotropic) yield stress fluid (see [49-50]).

The clay paste is a suspension of kaolin (*Speswhite, Imerys*) (volume fraction 27%, weight fraction 50%) in demineralized water. The kaolin particles are plate-like with an equivalent spherical diameter of $2\mu\text{m}$. A homogeneous suspension is rapidly obtained by hand mixing the powder and water for a few minutes. Its pH was 5 and its density is 1440 kg m^{-3} . In such a system colloidal interactions are

negligible. The rheological behavior of this material type is essentially that of a non-thixotropic yield stress fluid (see [51]).

For each material type reproducibility of the fluid behavior was confirmed by comparison of flow curve measurements before and after each series of extrusion experiments with a new batch of material.

3.2 Shear rheometry

We characterized the kaolin paste and the emulsion by shear rheometry, with a stress controlled *Malvern Kinexus pro+* rheometer equipped with parallel disks geometry of diameter 50 mm with rough surfaces and a gap of 1 mm. To assess the behavior in the liquid regime, we imposed increasing then decreasing stress ramps over 2 min, after a preshear at 10 s^{-1} during 20 s. The corresponding stress vs shear rate curves rather well superimpose beyond some critical stress; the slight remaining differences can be due to some evolution of edge effects. Thus thixotropic effects are negligible, and we retain the decreasing curve as representing the behavior in the liquid regime in steady state (see Figure 3). Under these conditions, the material yield stress is a unique parameter of the material whose value may be estimated from the plateau level in the flow curve. Systematic creep tests at different stress values were also carried out starting from rest (see Figure 4). In such tests, the deformation vs time curve tends to saturate for a stress below a critical value while it tends to increase at a constant rate for a larger stress (see e.g. [52]). Note that in contrast with the other creep curves which rapidly reach a deformation plateau, for the last creep flow curve in the saturation regime (i.e. for a stress just below the yield stress (see inset of Figure 4)), the deformation slowly increases, but the corresponding apparent shear rate continuously decreases in time so that no steady state is reached. This means that the liquid regime is not reached yet for this stress value. This critical stress marking the transition between the solid and the liquid regime is then associated with a stress just above this value. It is found to be very close to the yield stress value identified from the plateau in the flow curve (see Figure 3). Finally, in the next steps we directly determined the (simple shear) yield stress value of the material as the value of the parameter τ_c in the Herschel-Bulkley model fitted to the down ramp flow curve data (see Figure 3). The uncertainty on rheometrical tests, and thus on the rheological parameter values provided, which may be deduced from a repetition of similar tests, can be considered in our case to be about 5%.

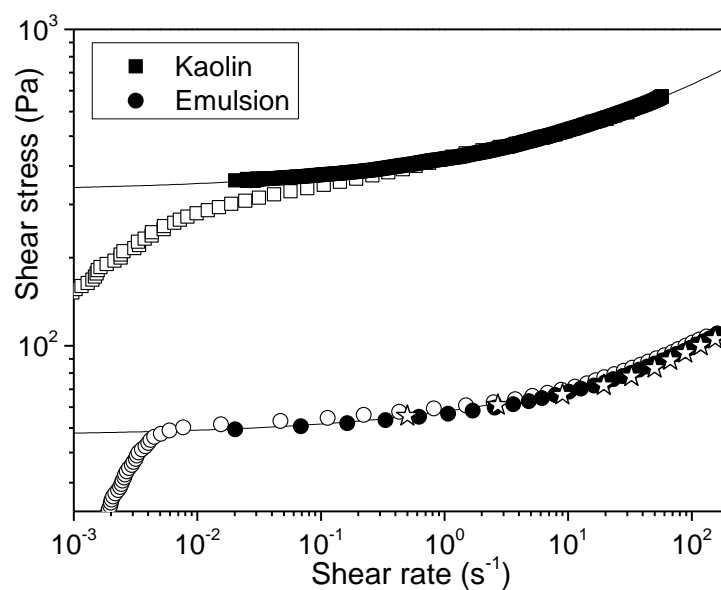


Figure 3: Flow curve of each material type obtained from up and down ramp test (open symbols for ramp up – filled symbols for ramp down) and steady state flow in the liquid regime during creep tests (stars) for the emulsion. The continuous lines correspond to the Herschel-Bulkley model in simple shear fitted to data (equation (14)) with $\tau_c = 309 \text{ Pa}$, $k = 78 \text{ Pa s}^n$ and $n = 1/3$ for the kaolin suspension, and $\tau_c = 52 \text{ Pa}$, $k = 10.75 \text{ Pa s}^n$ and $n = 1/3$ for the emulsion.

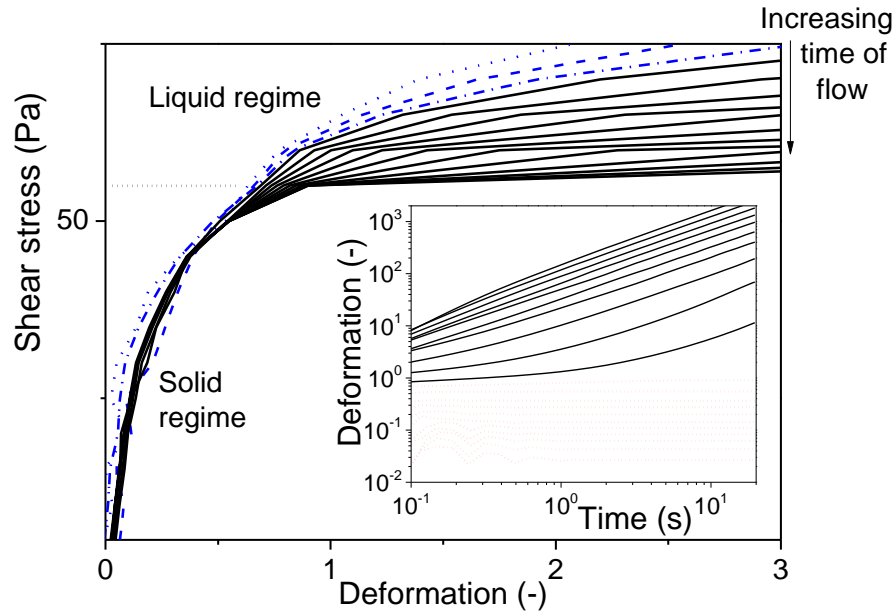


Figure 4: Creep tests in simple shear for the emulsion: application of different stress values to the material initially at rest for each new value. The resulting deformation vs time is represented in the inset for the different stress values: from bottom to top every 5 Pa starting from 5 Pa. The red dotted lines correspond to the solid regime, the continuous black lines to the liquid regime. The data in the main graph correspond to the same tests where the data have been represented in terms of shear stress vs deformation obtained at different times during these creep tests: (from top to bottom) 0.5, 0.7, 0.9, 0.11, 0.2, 0.3, 0.5, 0.8, 1.2, 2, 3, 5, 7, 9 s. The first curves, which do not yet superimpose to the final (stopped) state in the solid regime are drawn in blue. The approximate position of the yield stress is shown by a black dotted line.

3.3 Set up for extensional flow

The setup to induce an extensional flow is a traction machine (INSTRON) that has been adapted to be used as an extruder (see Figure 5a). The upper part is a piston, which can be moved vertically at a velocity controlled within 0.2%. This piston moves in a 12 cm diameter cylinder, with a nozzle at its bottom. The contact between the piston and the inner cylinder surface is maintained with the help of a seal, which precludes any leakage. The cylinder is initially filled with the material, then the piston is moved at a given velocity which extrudes the material through the nozzle (see Figure 5b). For this study, three cylindrical nozzles were used, with the following diameters and lengths: 1 and 3 cm; 2 and 6 cm; 4 and 12 cm. The mean velocity of the extrudate was varied from $0.036 \text{ mm} \cdot \text{s}^{-1}$ to $36 \text{ mm} \cdot \text{s}^{-1}$.

3.4 Imaging

Each extrusion test is filmed with high resolution (1080*1920) at 60 fps with a Panasonic Lumix FZ82, from the beginning of the exit of the filament from the nozzle to its breakage. A Python computer code was written to extract, from the video, data in terms of the extrudate radius as a function of the vertical position Z from its tip and time t , i.e. $R(Z, t)$ (see Figure 5c). Note that for all data except when mentioned we measured the droplet diameter and divided by two to deduce R . A second part of the same code uses discretized expressions of the theoretical formulas (see below) giving the strain rate and the stress along the filament at each time during the extrusion.

More precisely, the raw data are a series of images in grey level, with a minimum precision of about 200 pixels per cm. Different treatments are then applied to these images (noise removal, thresholding) to get a binary image in which the interface between the white and black areas corresponds to the fluid-air interface. The data on the radii (distance of this interface with regards to the central axis) are then further smoothed using a simple moving average (over 10 points). This smoothing allows for an enhanced precision, yet keeping the set of values of R discrete. Finally the derivative of R with regards to the time and the distance along the axis are performed with a centered finite difference.

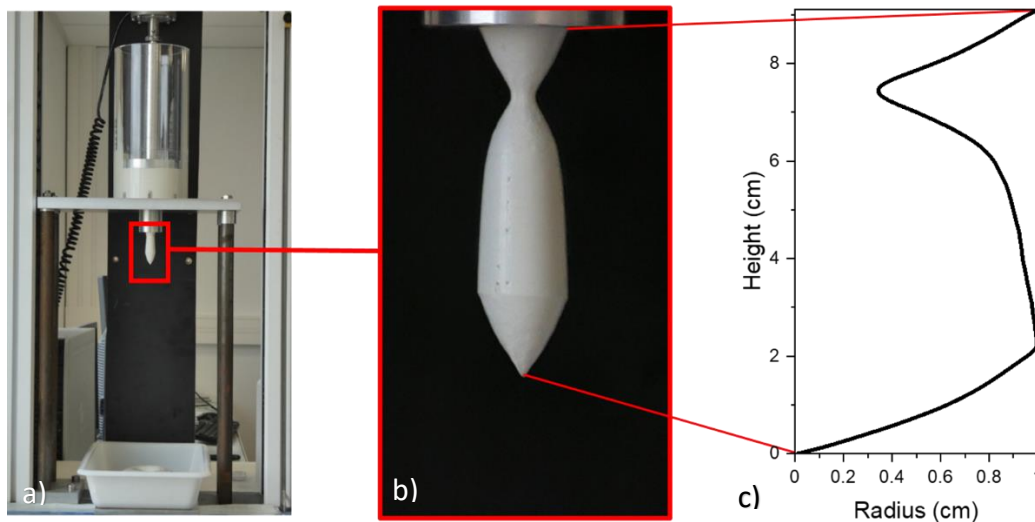


Figure 5. Principle of measurements during elongational test : a) Traction machine extruding (at 3.6 mm/s) the material (here kaolin suspension) through a cylindrical nozzle; b) Image of the filament; c) Radius vs height extracted from this image.

4. Results and discussion

4.1 Characteristics of the filament

The basic data of our extrusion tests is the set of the whole shapes of the filament ($R(Z, t)$) at different times between the initial one (breakage of the previous drop) and the time at which the current drop breaks. Examples are shown in Figure 6 which present the typical qualitative characteristics of the extrudate deformation and flow in our range of tests. Note that, in these figures, the profiles are somewhat distorted as the scales used for the radius and the height are different. Also note that in our tests we did not notice any swelling of the extrudate at its exit, but data very close to this exit (see top part of the profiles in Figure 5) could not be obtained as this region was darkened in our pictures by the shadow of the nozzle (this problem essentially appear after thresholding).

Although the free surface of the kaolin extrudate in the flowing region appears rougher than that of the emulsion, the results in terms of the evolution of the profile shapes for the kaolin suspension and

the emulsion are qualitatively analogous (see Figure 6). Obviously, differences can nevertheless be observed concerning the exact timing and shape of the deformation or flow regions, which can be discussed relevantly only through a quantitative analysis (see below). The roughness effect for kaolin is more pronounced at low extrusion velocities, and it will not be visible in the profiles of the drop presented below due to the smoothing procedure for data analysis. This roughness might be due to some “surface instability” which might be due to the specific structure of the kaolin suspension, made of a high concentration of large platelets, which could tend to form some arrangements along the interface during its extension. As it seems to concern only a very thin layer along the surface we consider this is not a fluid mechanics instability, and the bulk flow is negligible affected.

The first aspect of the extrudate, i.e. just after breakage of the previous drop, is conical (see Figure 1). This results from the deformation and/or flow induced by the weight of material acting on the sample part situated between the thinner point and the fluid in the die, whose diameter is imposed. Then, as the extrudate advances, we can observe from the successive profiles (see Figure 6) a region of slight deformation just above the conical region, where the profiles finally superimpose. In the region above, the thickness of the extrudate decreases more rapidly and continuously.

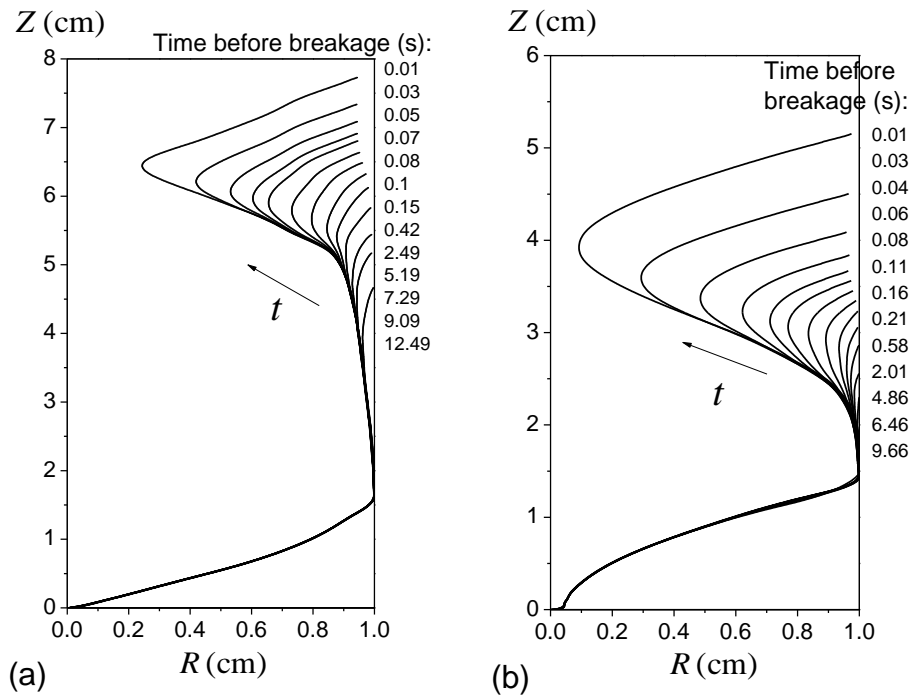


Figure 6. Profiles of radius vs height for extrudates of kaolin suspension (a) and emulsion (b) at different times during extrusion through a 2 cm nozzle diameter for the tests shown in Figure 1. Here the profiles have been drawn in a referential where 0 is the position of droplet bottom.

Since in this filament elongation a different normal stress is applied at different positions along the filament axis, it is instructive to compare the corresponding evolution of the local deformation in time to the evolution of the shear deformation when applying different stress values in a simple shear experiment under controlled shear stress. In the latter case, i.e. when applying a series of creep tests at different (shear) stress levels to a yield stress fluid (see inset of Figure 4), a short time after the application of each stress, the deformation is small in any case; some time later, for a stress below the yield stress, the deformation tends to saturate, while, for a larger stress, the deformation continuously increases; later on, in the first region (i.e. below the yield stress), the deformation is constant, while it linearly increases in time in the other region (i.e. above the yield stress) at a rate increasing with the

stress value (see inset of Figure 4). If we now represent the evolution in time of the stress vs deformation curves, we now see a solid region in which the deformation tends to a finite value, and a liquid region where it continuously increases in time. This leads to successive profiles (see Figure 4) with a slope breakage at the solid-liquid transition point.

The qualitative features for apparent deformation along the filament (deformation roughly estimated from the ratio of the initial radius to the current radius) resemble the trends observed for such a series of shear creep tests: neglecting the region, just below the yield stress, associated with the slow residual flow in the solid regime (see Section 3.2), we can identify mainly two branches, one for the solid regime and the other for the liquid regime; a slope breakage progressively appears between these two branches, which likely corresponds to the transition between the solid and the liquid regime (see Figure 6). In fact, it is worth noting that the situation for the elongational test is more complex since the normal stress applied on a given layer of material increases with the deformation and the time of flow is much more limited. We nevertheless suggest to interpret the apparent slope breakage in the same way, by considering that this position corresponds to the point of transition between the solid and the liquid regions. Obviously, as usual for any type of experiment for determining the yielding point, it is difficult to distinguish precisely its exact value as it corresponds to a region below which the deformation is finite, and a region where the material, in theory, flows at an infinitely small rate.

This approach essentially allows us to determine the liquid region, in which we are going to further analyze the flow characteristics. We could expect this would provide also an estimation of the elongational yield stress. However, the situation is not so simple as we cannot be sure that the flow in the region is a pure elongational one. Actually, in the next section we will see that this is not at all the case, which explains that using directly the apparent normal stress observed at the slope breakage would yield significantly smaller values than the elongational yield stress found through a more careful approach (see below).

Let us now consider the question of the reproducibility of such data. For a typical succession of droplets in the same test the profiles at different times during flow and breakage appear to be very close except just before breakage for the emulsion, and somewhat more scattered for the kaolin suspension (see Appendix 2). However the overall shape evolution is similar. Also note that from such data we can see that the differences between the two sides of the profiles for the emulsion fall in the same range as the fluctuations observed from successive droplets (see Appendix 2). Besides, we can note that the repeatability of the experiments for a given set of parameters was good, and the variability of the droplets profiles from one test to another was similar to that observed for a succession of droplets during the same test. Averaging the successive profile points for each radial distance to get a more robust shape does not seem relevant as the profile differences have a 2D nature. Moreover, the differences observed in the free surface profiles for different droplets or different tests do not directly provide some indication on the uncertainty on the determination of the constitutive equation. Indeed, for example some local “accident” in the process leading to a deviation from the expected theoretical shape of the filament otherwise, will not directly induce a corresponding defect in the deduced constitutive equation. Actually, this deviation will induce a deviation on the local stress that will be taken in our approach which relies on the full shape measurements. Thus, in order to relevantly appreciate the uncertainty or the reproducibility of this rheometrical approach, it is necessary to compare directly the resulting constitutive equation data.

4.2 Rheological analysis of flow characteristics

We now analyze these profiles with the help of theory presented above. Here we focus on the part of filament profile situated below the pinch-off, as in this region the material clearly exhibits a solid region and the liquid region. The flow characteristics of the top part of the extrudate, located between the filament pinch-off and the nozzle, seem somewhat more complex. In particular, due to the attachment

of the filament to the die exit the solid-liquid transition cannot be easily distinguished. A further careful analysis of this region might provide useful information, which is left for future work.

Since the fluid elements in the solid region are submitted to some given stress it should *a priori* be possible to extract some relationship between normal stress and strain in elongation from the drop profiles obtained after stabilization in the solid regime. However, various effects preclude a straightforward analysis of the data to get this relationship. In particular, we do not control the exact initial size of the filament to be taken into account as a reference to compute the deformation: the filament diameter may be slightly affected by the exit from the die, and, just after it exits, it is submitted to some significant stress before drop breakage, which leads to the cone formation. As a consequence, here we focus on the data obtained in what we distinguished as the liquid regime.

Analyzing the profiles (see Figure 5) of the filament at each time during flow in the liquid regime makes it possible to deduce an “apparent flow curve” of the material (see Figure 7), representing the instantaneous relationship between the normal stress and the strain rate along the sample profile whatever the flow characteristics, i.e. even under conditions for which the flow is not purely elongational. We then can see that these successive apparent flow curves progressively shift towards higher shear rates, with some of them (for the kaolin suspension) apparently superimposing at the highest shear rates. Since in the very first times the deformation beyond yielding is very limited in the region of small strain rate the above results could be interpreted as some progressive behavior transition to the steady state liquid behavior. The exact behavior of yield stress fluids during this transient regime constitutes an open question. In the following we show that these different apparent flow curves can more likely be attributed to the non-normal strain rate or stress components. As a corollary this tends to suggest that under these flow conditions the transition from solid behavior to steady state liquid behavior for these fluids is almost instantaneous beyond the critical deformation.

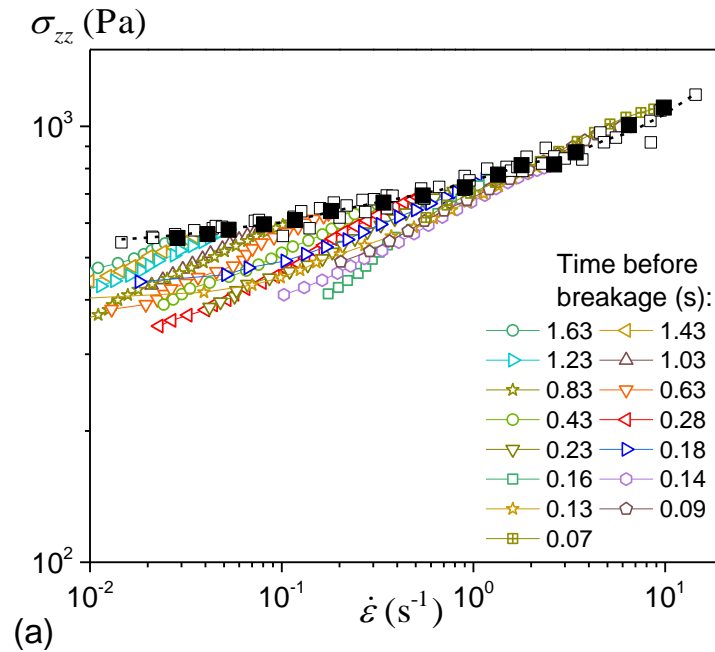
Looking at the values of $\tan i$ and $\beta = (R/4\dot{\epsilon})(\partial\dot{\epsilon}/\partial z)$ for these data, we observe that these two variables decrease as the normal stress increases (see Figure 8). More precisely, along each curve (derived from the analysis of the flow at a given point), $\tan i$ and β are respectively larger than 0.1 and 0.3, and finally become smaller for the very last points (except for 3 points for the emulsion, for which β is between 0.4 and 0.5), i.e. for the largest stress. This means that, for several data points along these apparent flow curves, the components of the stress tensor other than σ_{zz} , and the shear rate, are significant and our analysis relying on the assumption of a pure elongational flow is not valid. Thus, it is misleading to interpret an apparent flow curve (deduced from a filament profile at a given time) as giving the shape of the “elongational” flow curve, since its shape is affected by the variable impact, with the stress increase, of the non-purely elongational components of the stress and strain rate tensors. In particular these apparent curves have a steeper slope for larger initial filament radius (data not shown here), which results from the fact that the position of breakage does not vary much with the initial radius, so that we have a steeper slope of the profile from the solid region to the pinch off point. However, as we will see below these different apparent flow curves “converge” to the same point in the pinch off region.

Actually, this impact of the other stress and strain rate tensor components decreases as the stress increases, and tends to become negligible when $\tan i$ and β reach small values. Finally, it appears that almost all the last data points (i.e. for the largest stress) along each of these curves values (larger filled symbols in Figure 8) correspond to a situation for which the non-normal components can be neglected, and we can consider them as parts of the “effective flow curve” in elongation, i.e. associated with pure elongational flow. This means that we finally essentially retain the information from the pinch off region of the drop, while the other regions provide only rough approximations of the effective elongational behavior of the fluid. By the way, we can remark that by doing so we retain data in a region for which our basic theoretical assumption of uniform velocity in each section is certainly valid (see Section 2). Note that, since our criterion for the negligibility of the non-normal components is the same all along this final curve, i.e. at any strain rate, there is no particular range for which we can

expect non-elongational effects to be at the origin of some larger uncertainty on the flow curve obtained here.

At last, we can check that taking into account the acceleration term is critical. Without this term the last apparent flow curves, i.e. in the last times of flow before filament breakage, significantly depart from the rest of the curves (see Appendix 3). They can differ by a stress factor as large as 2 from the master flow curve obtained otherwise. Also note that the second term of acceleration (associated to b) was less than 1% in that case, which confirms its negligibility.

Such elongation flow curves can be obtained from each drop, so that we can test the reproducibility of the results for successive drops of the same test. Typical results for four successive drops are shown in Figure 7, in which only a slight scatter may be observed. A similar conclusion is reached from the analysis of left and right profiles of the same drop, despite the instability noticed in the pictures (see Figure 1). We conclude that the uncertainty on the determination of the elongational flow curve under given conditions according to our procedure is about 5%. Finally we choose to fit some average elongational flow curve with a best fit procedure on such data obtained from a series of successive drops, and consider this as the effective flow curve associated with the test. Thus, we obtain the effective flow curve of the material as deduced from a test under given conditions. Note that, since this flow curve has a shape typical of a yield stress fluid behavior, i.e. with a plateau at low strain rates, the yield stress of the material in elongation is then very close to the lowest normal stress of this flow curve. It thus significantly differs from the critical stress value associated with the slope breakage in the profiles (see Figure 6), which in fact corresponds to the lowest stress value observed in the apparent flow curves.



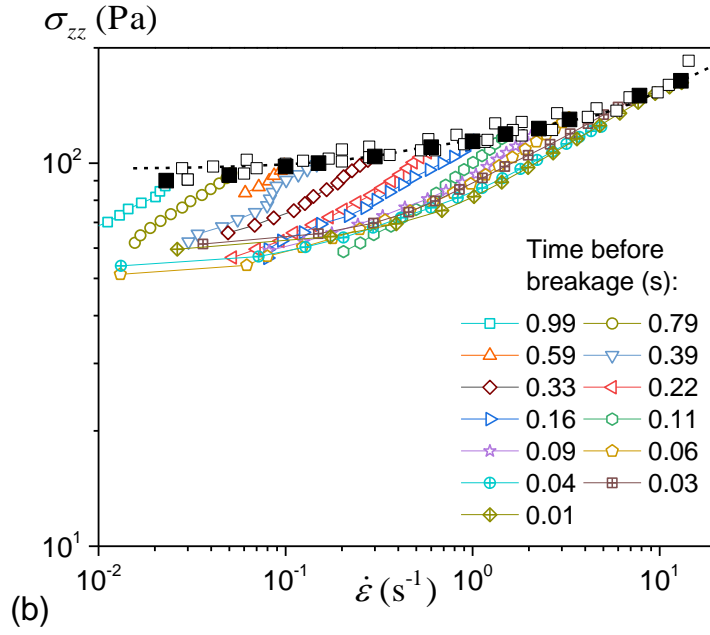
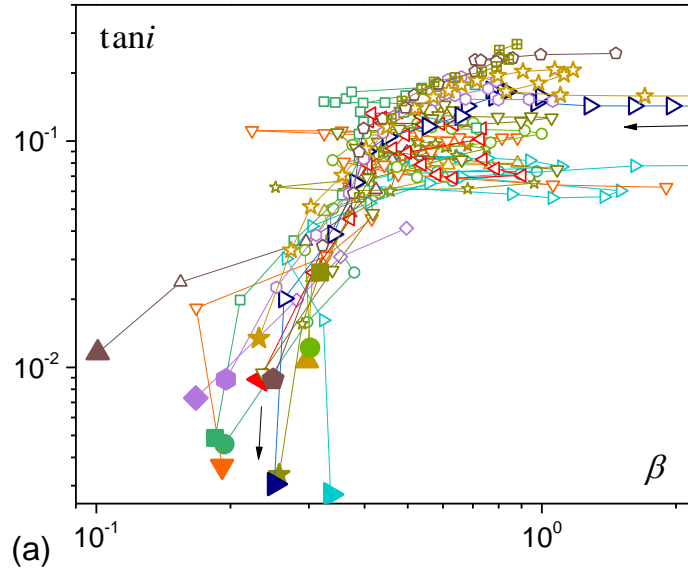


Figure 7. Apparent flow curves in terms of normal stress vs elongation strain rate along the sample at different times during filament deformation in the liquid regime for: (a) the kaolin suspension for a velocity of 0.36 mm s^{-1} and a die diameter of 4 cm , (b) the emulsion at a velocity of 0.9 mm s^{-1} and die diameter of 2 cm , at different times from the previous droplet breakage (see caption in graph). The large black filled square symbols correspond to the data points the closest to a pure elongational flow. The large black open squares correspond to the same situation for three other successive drops during the same test.



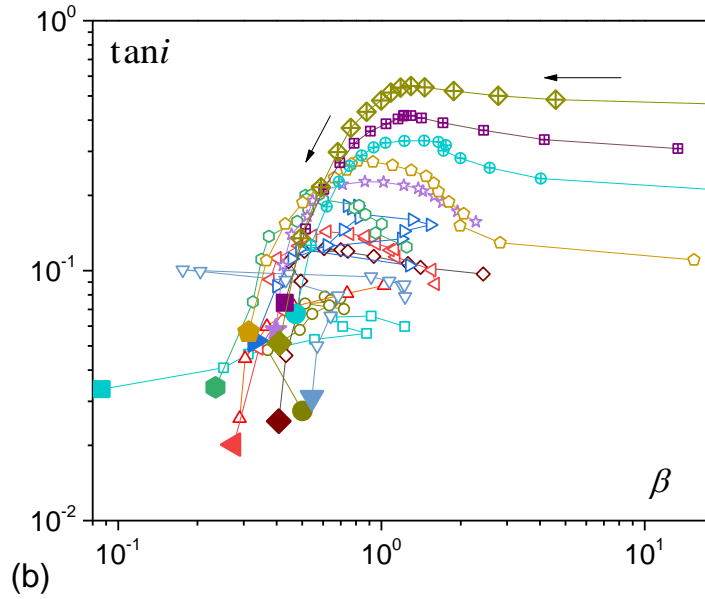


Figure 8. Slope of the sample profile vs ratio of shear to elongational rate components ($\tan i$ vs $\beta = (R/4\dot{\epsilon})(\partial\dot{\epsilon}/\partial z)$) corresponding to the tests of Figure 7 (same symbols) for the kaolin suspension (a) and the emulsion (b). The arrows shows the direction of increase of the normal stress for a given time for one set of data (larger symbols) associated with a profile at a given time. The last data points, retained for the effective flow curve, are represented by larger, filled symbols.

4.3 Discussion

We can now gather all the flow curve data obtained through this procedure in the same graph, i.e. for each experiment we now keep only the data points identified as corresponding to pure elongational flow according to the technique described in the previous section, i.e. the effective flow curve data. For different diameters and a velocity varied over three decades a master flow curve is obtained for the kaolin suspension with an uncertainty of 12%, and a master flow curve is obtained for the emulsion with an uncertainty of 8% (see Figure 9). The superimposition of a wide set of data obtained under different conditions and at different times during the flow demonstrate that a robust, consistent rheological behavior is extracted from these tests.

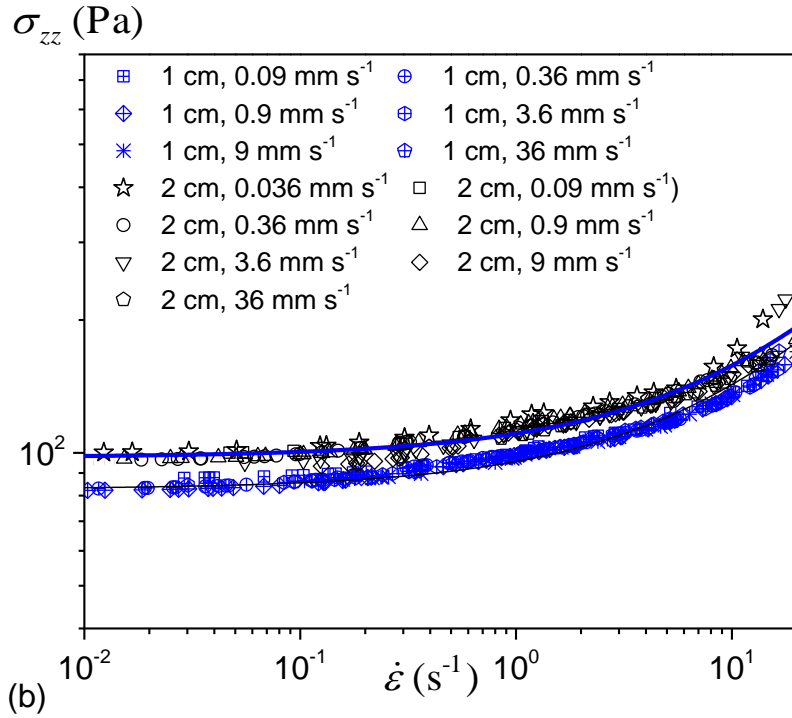
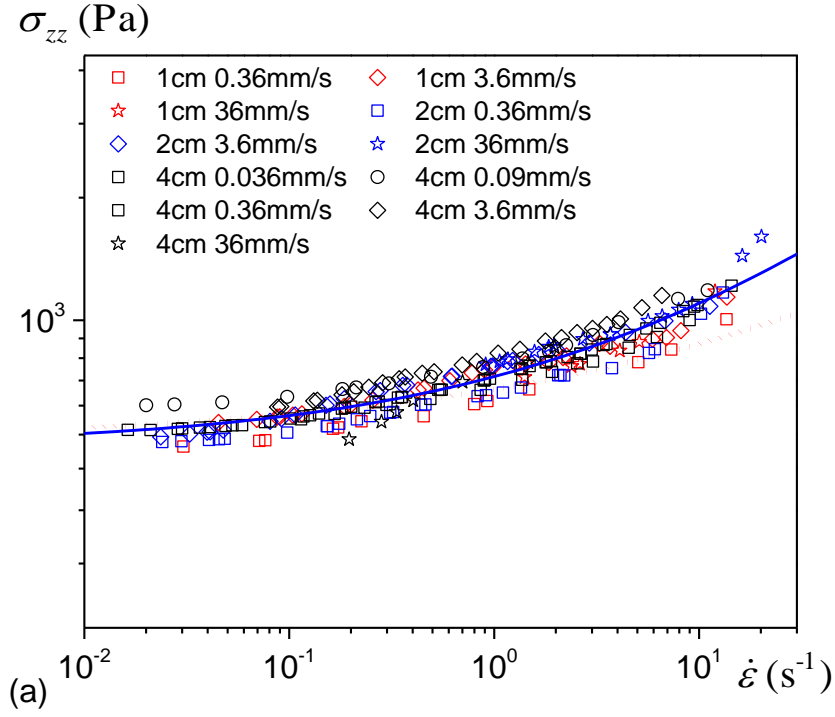


Figure 9: Flow curves in elongational flow for the kaolin suspension (a) and the emulsion (b) under different conditions (see legend). The red dotted lines corresponds to the expression derived from the standard 3D Herschel-Bulkley model in pure elongational flow (i.e. equation (16)) using the rheological parameters determined in simple shear (see Figure 3). The thick continuous blue lines correspond to the best fit of a Herschel-Bulkley model for the elongation flow (i.e. equation 16), with parameters: $\tau_c = 299$ Pa ,

$k = 105 \text{ Pa s}^n$ and $n = 0.4$ for the kaolin, and $\tau_c = 56.4 \text{ Pa}$, $k = 5.1 \text{ Pa s}^n$ and $n = 0.67$. For the emulsion this fit was done on the data for a 2 cm diameter; the thin black line is this best fit minus 15 Pa on the stress (i.e. $\tau_c = 48 \text{ Pa}$, $k = 5.1 \text{ Pa s}^n$ and $n = 0.67$).

For the emulsion one may also distinguish two master curves with a smaller uncertainty (3.5%) for each of the two diameter tested (see Figure 9b), which suggests that here the diameter has some impact on the data. Actually, this difference essentially takes the form of a stress shift, i.e. the master curve for a 1 cm diameter is approximately similar to the master curve for a 2 cm diameter by adding a constant stress value (15 Pa) to the normal stress (see Figure 9b). This difference could essentially come from surface tension effects. Indeed, for all the tests with the kaolin suspension we have $\sigma_c R_0 / \gamma > 40$, which is consistent with the fact that a single master curve is obtained, i.e. capillary effects are negligible and the constitutive equation is independent of the diameter. For the emulsion we have $\tau_c R_0 / \gamma > 13$ for the tests with a 2 cm diameter, and we can consider that capillary effects play a minor effect, but for a 1 cm diameter $\sigma_c R_0 / \gamma$ reaches values as low as 6.4, so that capillary effects may affect the results in some extent. We are unable to more precisely quantify these effects, and here we will just consider, in consistency with this qualitative analysis, that the data for a 2 cm diameter with the emulsion are not affected by capillary effects and thus well reflect the material behavior.

It is now of interest to compare the results concerning the rheological behavior in elongational flow to those observed in simple shear. In the latter case the Herschel-Bulkley model appears to very well represent the data (see Figure 3). In simple shear this model expresses as:

$$\tau > \tau_c \Rightarrow \tau = \tau_c + k \dot{\gamma}^n \quad (14)$$

where τ_c is the yield stress, k and n materials parameters, and τ and $\dot{\gamma}$ respectively the shear stress and shear rate amplitudes. The 3D form of this constitutive equation has been the subject of discussions but the simplest form initially proposed by Oldroyd [15] is as follows:

$$\sqrt{T_{II}} > \tau_c \Rightarrow \boldsymbol{\Sigma} = -p\mathbf{I} + \tau_c \frac{\mathbf{D}}{\sqrt{D_{II}}} + \left(\frac{2^n k}{(D_{II})^{(1-n)/2}} \right) \mathbf{D} \quad (15)$$

in which \mathbf{I} is the identity tensor, $T_{II} = \frac{1}{2} \text{tr} \mathbf{T}^2$ and $D_{II} = \frac{1}{2} \text{tr} \mathbf{D}^2$ are the second invariants of \mathbf{T} and \mathbf{D} , where \mathbf{T} is the extra-stress tensor defined as $\boldsymbol{\Sigma}(Z, t) = -p\mathbf{I} + \mathbf{T}$ with $\text{tr} \mathbf{T} = 0$.

For a purely elongational flow, we have $D_{II} = \frac{3}{4} \dot{\epsilon}^2$ and $T_{II} = \frac{\sigma_{zz}^2}{3}$, so that the constitutive equation in the liquid regime writes:

$$|\sigma_{zz}| > \sqrt{3} \tau_c \Rightarrow \sigma_{zz} = \sqrt{3} \left[\tau_c + k \left| \sqrt{3} \dot{\epsilon} \right|^n \right] \quad (16)$$

It appears that this model very well predicts the elongational yield stress observed in our experiments: the stress plateau indeed corresponds to the $\sqrt{3} \tau_c$ prediction of (17) (see Figure 9). In terms of normal stress we get for the kaolin suspension 517 Pa from our filament tests, whereas the prediction from simple shear tests and the standard 3D formulation is 535 Pa. For the emulsion we get 97.7 Pa from our filament tests with the 2 cm die, and 84 Pa with the 1 cm die, while the theoretical prediction is 90 Pa. Such differences fall in the possible range of uncertainty. Thus our results confirm the validity of the standard model.

This conclusion is in agreement with results from inspection of capillary forces around filament breakage to estimate the elongational yield stress [26-27]. On another side, the present results appear to be in contradiction with the estimations from recent measurements under different well-controlled conditions, i.e. extension between solid plates with wall slip [31], or cross-flow extensional rheometry [33]. It seems difficult to explain the origin of this difference, in particular to distinguish whether it comes from the flow conditions under consideration (bulk flow or filament stretching free of other constraints?), or some specificity of the rheological behavior of the material, but we can at least remark that we have here more straightforward and more precise data over several decades of strain rates, and for a range of filament radii.

Interestingly, here we can look in more details at the form of the flow curve in elongational flow over several decades of strain rates, and for example compare it with the prediction (i.e. equation (16)) of the standard 3D model. We can see that the qualitative aspect is the same as that expected from a Herschel-Bulkley model, i.e. a plateau at low strain rates then a progressive increase of the normal stress for increasing strain rates. However, the exact theoretical flow curve (equation 16) does not well represent the data, i.e. it underestimates the stress at strain rates larger than a few s^{-1} (see Figure 9). This means that the stress increases slightly faster with strain rate than expected from this model. The best fit procedure gives a parameter a value for n equal to 0.4 for the kaolin suspension and 0.67 for the emulsion (see Figure 9), whereas the simple shear tests gives 0.33. As far as we know no simple constitutive equation has been proposed which predicts such a trend.

Conclusion

We here provide a complete rheometrical approach of the elongational flow of yield stress fluids, with simple technical means, which aims at determining the constitutive equation of the material in elongation. The transition between the solid and the liquid regime can be properly determined, which provides the elongational yield stress of the material. Our detailed analysis of the flow then essentially concerns the liquid regime, as the deformations in the solid regime in some region of the material are affected by the flow of the drop when it was still in contact with the previous drop. The flow in the liquid regime is nevertheless not a pure elongational flow, due to the large gradient of filament thickness. From the identification of the pure elongational region at different times during flow for a series of tests under different flow rates and filament diameters we were able to extract the constitutive equation in elongation in the liquid regime of a yield stress fluid, without a priori assumptions on the material behavior, i.e. as for a standard rheometrical approach.

We finally were able to properly determine the elongational yield stress of two typical yield stress materials. It appears that, in contrast with certain previous results under other conditions, but in agreement with others (see Introduction), this value is that predicted by the basic Oldroyd model. The form of the constitutive equation appears to be close to that expected from the Herschel-Bulkley model, except that the exponent might be slightly larger than in simple shear. Thus, our direct measurement of the constitutive equation in elongation provides, at least for the two materials tested here, relatively simple results by comparison with some more sophisticated or indirect measurements.

Appendix 1: Impact of the shear rate component on the constitutive equation in elongational flow

Taking into account the shear rate component we now have $D_{II} = \frac{1}{2} \text{tr} \mathbf{D}^2 = \frac{3}{4} \dot{\epsilon}^2 [1 + 4\beta^2/3]$. In the case of the Oldroyd 3D expression of the Herschel-Bulkley model, we deduce

$$\sigma_{zz} = \frac{\sqrt{3}}{\alpha} \left[\tau_c + \left| \sqrt{3} \alpha \dot{\epsilon} \right|^n \right]$$

in which $\alpha = \sqrt{1 + 4\beta^2/3}$

Thus, if $\beta < 0.4$, the shear component affects the stress and the strain rate by less than 10% ($\alpha < 1.1$). For $\beta = 0.5$ the impact of the shear component is equal to 15%.

Appendix 2: Reproducibility of droplet shape.

Here we present the shape for a succession of three droplets in the same test, for the different materials and compare the profiles observed at different times during the flow then breakage (see Figure 10 a,b. For the emulsion we also compare the profiles obtained when measuring the radius from the left or right side only.

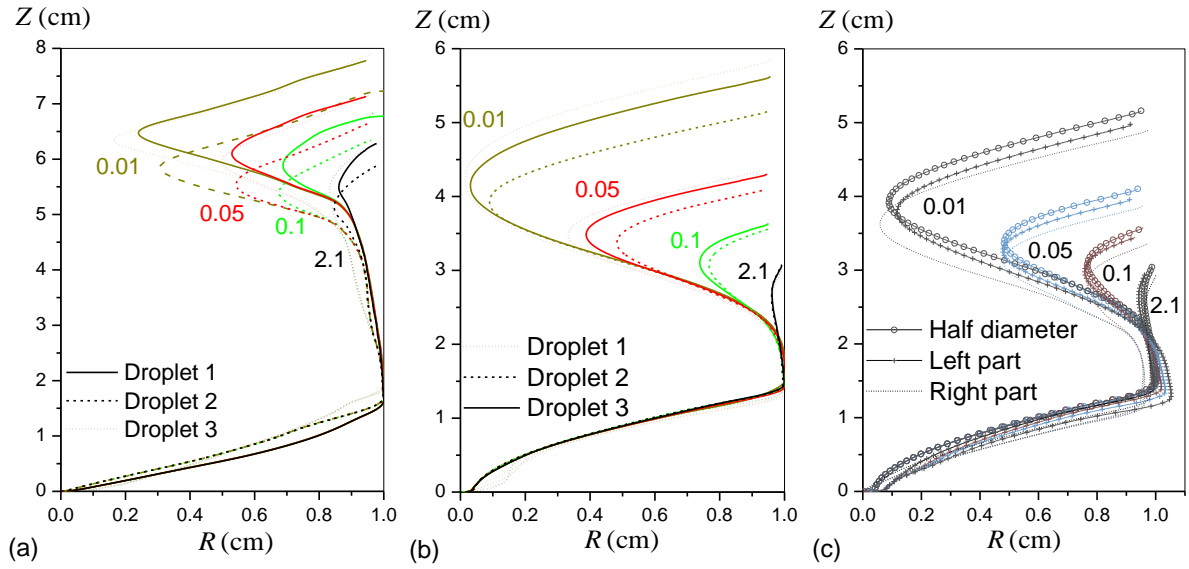


Figure 10: Profiles at different times (lines of different colors; times indicated in seconds in the graphs) for three successive droplets (different line characteristics) in the same test with kaolin suspension (a) and emulsion (b), and for the right and left side of an emulsion droplet, and half its diameter (standard measurement in this paper) (c).

Appendix 3. Impact of the acceleration term on the apparent flow curve.

Figure 11 shows the difference between the apparent flow curves deduced directly from the profile analysis by considering only the gravity term in the stress and the apparent flow curve computed by taking into account also the acceleration term.

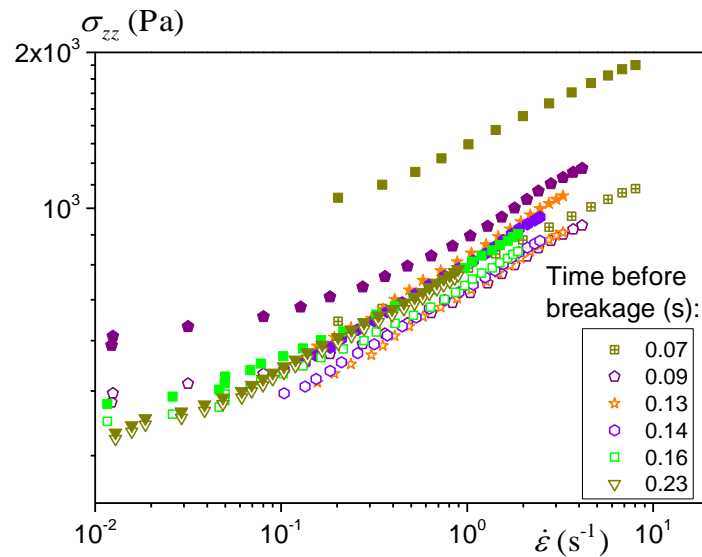


Figure 11: Apparent flow curves for the test of Figure 7a at different times before breakage, taking (open symbols) or not (filled symbols) the acceleration term.

References

- [1] Townsend, J. M., E. C. Beck, S. H. Gehrke, C. J. Berkland, M. S. Detamore, "Flow behavior prior to crosslinking: the need for precursor rheology for placement of hydrogels in medical applications and for 3D bioprinting", *Prog. Polym. Sci.*, **91**, 126-140 (2019)
- [2] M'Barki A., L. Bocquet, A. Stevenson, « Linking rheology and printability for dense and strong ceramics by direct ink writing », *Scientific Reports*, **7**, 6017 (2017)
- [3] Jeong H., S.-J. Han, S.-H. Choi, Y. J. Lee, S. T. Yi, K. S. Kim, "Rheological property criteria for buildable 3D printing concrete", *Materials*, **12**, 657 (2019)
- [4] Mechtcherine V., F. P. Bos, A. Perrot, W. R. Leal da Silva, V. N. Nerella, S. Fataei, R. J. M. Wolfs, M. Sonebi, N. Roussel, « Extrusion-based additive manufacturing with cement-based materials – Production steps, processes, and their underlying physics : a review », *Cement and Concrete Research*, **132**, 106037 (2020)
- [5] Daalkhaijav U., O. D. Yirmibesoglu, S. Walker, Y. Menguc, "Rheological Modification of Liquid Metal for Additive Manufacturing of Stretchable Electronics", *Adv. Mat. Technol*, **3**, 1700351 (2018)
- [6] Tiwari M. K., A. V. Bazilevsky, A. L. Yarin, C. M. Megaridis, "Elongational and shear rheology of carbon nanotube suspensions", *Rheol. Acta*, **48**, 597-609 (2009)
- [7] Mackay, M. E., "The importance of rheological behavior in the additive manufacturing technique material extrusion", *J. Rheol.*, **62**, 1549 (2018)
- [8] Nelson A. Z., K. S. Schweizer, B. M. Rauzan, R. G. Nuzzo, J. Vermant, R. H. Ewoldt, "Designing and transforming yield-stress fluids", *Current Opinion in Solid State and Materials Science*, **23**, 100758 (2019)
- [9] Coussot P., L. Tocquer, C. Lanos, G. Ovarlez, "Macroscopic vs local rheology of yield stress fluids", *Journal of Non-Newtonian Fluid Mechanics*, **158**, 85-90 (2009)

- [10] Ovarlez G., S. Rodts, X. Chateau, P. Coussot, "Phenomenology and physical origin of shear-localization and shear-banding in complex fluids", *Rheologica Acta*, **48**, 831 – 844 (2009)
- [11] Ovarlez G., S. Cohen-Addad, K. Krishan, J. Goyon, P. Coussot, "On the existence of a simple yield stress fluid behavior", *J. Non-Newt. Fluid Mech.*, **193**, 68-79 (2013)
- [12] Balmforth N. J., I. A. Frigaard, G. Ovarlez, "Yielding to stress: Recent developments in viscoplastic fluid mechanics", *Ann. Rev. Fluid Mech.*, **46**, 121-146 (2014)
- [13] Bingham E. C., "An investigation of the laws of plastic flow", *Bulletin of the Bureau of Standards*, **13**, 309-353 (1916)
- [14] Herschel W. H., R. Bulkley, Consistency measurements of rubber-benzol solutions, *Kolloid-Zeitschrift*, **39**, 291-300 (1926)
- [15] Oldroyd J. G., "A rational formulation of the equations of plastic flow for a Bingham solid", *Proc. Cambridge Philosophical Society*, **43**, 100-105 (1947)
- [16] Hohenemser K., W. Prager, "Über die ansätze der mechanik isotroper continua », *Zeitschrift für Angewandte Mathematik und Mechanik*, **12**, 216-226 (1932)
- [17] Bird R. B., G.C. Dai, B.J. Yarusso, "The rheology and flow of viscoplastic materials", *Rev. Chem. Eng.*, **1**, 1-70 (1983)
- [18] Coussot P., *Rheometry of pastes, suspensions and granular materials*, (Wiley, New York, 2005)
- [19] Saramito P., "A new constitutive equation for elastoviscoplastic fluid flows", *J. Non-Newt. Fluid Mech.*, **158**, 154-161 (2009)
- [20] Saramito P., "A new elastoviscoplastic model based on the Herschel-Bulkley viscoplastic model", *J. Non-Newt. Fluid Mech.*, **158**, 154-161 (2009)
- [21] Dimitriou C. J., R.H. Ewoldt, G. H. McKinley, "Describing and prescribing the constitutive response of yield stress fluids using large amplitude oscillatory shear stress (LAOStress)", *J. Rheol.*, **57**, 27-70 (2013)
- [22] Dimitriou C. J., G. H. McKinley, « A canonical framework for modeling elasto-viscoplasticity in complex fluids », *J. Non-Newt. Fluid Mech.*, **265**, 116-132 (2018)
- [23] Armstrong M. J., A. N. Beris, S. A. Rogers, N. J. Wagner, "Dynamic shear rheology of a thixotropic suspension: comparison of an improved structure-based model with large amplitude oscillatory shear experiments", *J. Rheol.*, **60**, 433-450 (2016)
- [24] Varchanis, S., G. Makrigiorgos, P. Moschopoulos, Y. Dimakopoulos, J. Tsamopoulos, "Modeling the rheology of thixotropic elasto-plastic materials", *J. Rheol.*, **63**, 609 (2019)
- [25] Niedzwiedz K., H. Buggisch, N. Willenbacher, "Extensional rheology of concentrated emulsions as probed by capillary breakup elongational rheometry (CaBER)", *Rheol. Acta*, **49**, 1103 (2010)
- [26] German G., V. Bertola, "Formation of viscoplastic drops by capillary breakup", *Phys. Fluids*, **22**, 033101 (2010)
- [27] Martinie L., H. Buggisch, N. Willenbacher, "Apparent elongational yield stress of soft matter", *J. Rheol.*, **57**, 627 (2013)
- [28] Sadek S. H., H.H. Najafabadi, F. J. Galindo-Rosales, "Capillary Breakup Extension ElectroRheometry (CaBEER)", *Journal of Rheology*, **64**, 43-54 (2020)
- [29] Sadek S. H., H.H. Najafabadi, F. J. Galindo-Rosales, "Capillary breakup extension magnetorheometry", *Journal of Rheology*, **64**, 55-65 (2020)
- [30] Boujlel J., P. Coussot, "Measuring the surface tension of yield stress fluids", *Soft Matter*, **9**, 5898 (2013)

- [31] Zhang X., O. Fadoul, E. Lorenceau, P. Coussot, "Yielding and flow of soft-jammed systems in elongation", *Phys. Rev. Lett.*, 120, 048001 (2018)
- [32] Louvet N., D. Bonn, H. Kellay, "Nonuniversality in the Pinch-Off of Yield Stress Fluids: Role of Nonlocal Rheology", *Phys. Rev. Lett.*, 113, 218302 (2014)
- [33] Varchanis S., S. J. Haward, C. C. Hopkins, A. Syrakos, A. Q. Shen, Y. Dimakopoulos, J. Tsamopoulos, "Transition between solid and liquid state of yield-stress fluids under purely extensional deformations", *PNAS*, 117, 12611-12617 (2020)
- [34] McKinley G. H., A. Tripathi, "How to extract the Newtonian viscosity from capillary breakup measurements in a filament rheometer", *J. Rheol.*, 44, 653-670 (2000)
- [35] Rodd L. E., T. P. Scott, J. J. Cooper-White, G. H. McKinley, "Capillary break-up rheometry of low-viscosity elastic fluids", *Appl. Rheol.*, 15, 12-27 (2005)
- [36] Yarin A. L., E. Zussman, A. Theron, "Elongational behavior of gelled propellant simulants", *J. Rheol.*, 48, 101-116 (2004)
- [37] Szabo P., "Transient filament stretching rheometer", *Rheol. Acta*, 36, 277-284 (1997)
- [38] Szabo P., G. H. McKinley, "Filament stretching rheometer: inertia compensation revisited", *Rheol. Acta*, 42, 269-272 (2003)
- [39] Tirtaatmadja V., T. Sridhar, "A filament stretching device for measurement of extensional viscosity", *Journal of Rheology*, 37, 1081-1102 (1993)
- [40] Anna S. L., G. H. McKinley, D. A. Nguyen, T. Sridhar, S. J. Muller, J. Huang, D. F. James, "An interlaboratory comparison of measurements from filament stretching rheometers using common test fluids", *J. Rheol.*, 45, 83-114 (2001)
- [41] McKinley G. H., T. Sridhar, "Filament-stretching rheometry of complex fluids", *Ann. Rev. Fluid Mech.*, 34, 375-415 (2002)
- [42] Barral Q., G. Ovarlez, X. Chateau, J. Boujlel, B. D. Rabideau, P. Coussot, "Adhesion of yield stress fluids", *Soft Matter* 6, 1343-1351 (2010)
- [43] Moschopoulos P., A. Syrakos, Y. Dimakopoulos, J. Tsamopoulos, Dynamics of viscoplastic filament stretching, *J. Non-Newt. Fluid Mech.*, 284, 104371 (2020)
- [44] McKinley G. H., "Visco-elasto-capillary thinning and break-up of complex fluids", *Rheology Reviews*, 1-48 (2005)
- [45] Henderson D. M., W.G. Pritchard, L. B. Smolka, "On the pinch-off of a pendant drop of viscous fluid", *Phys. Fluids*, 9, 3188-3200 (1997)
- [46] Sharma V., S. J. Haward, J. Serdy, B. Keshavarz, A. Soderlund, P. Threlfall-Holmes, G. H. McKinley, "The rheology of aqueous solutions of ethylhydroxy-ethyl cellulose (EHEC) and its hydrophobically modified analogue (hmEHEC): extensional flow response in capillary break-up, jetting (ROJER) and in a cross-slot extensional rheometer", *Soft Matter*, **11**, 3251-3270 (2015)
- [47] Coussot P., F. Gaulard, "Gravity flow instability of viscoplastic materials: The ketchup drip", *Phys. Rev. E*, 72, 031409 (2005)
- [48] Balmforth N.J., N. Dubash, A.C. Slim, "Extensional dynamics of viscoplastic filaments II: drips and bridges", *J. Non-Newt. Fluid Mech.*, 165, 1147 (2010)
- [49] Ovarlez G., S. Rodts, A. Ragouilliaux, P. Coussot, J. Goyon, A. Colin, "Wide-gap Couette flows of dense emulsions: Local concentration measurements, and comparison between macroscopic and local constitutive law measurements through magnetic resonance imaging", *Physical Review E* 78, 036307 (2008)

- [50] Zhang X., E. Lorenceau, T. Bourouina, P. Basset, T. Oerther, M. Ferrari, F. Rouyer, J. Goyon, P. Coussot, "Wall slip mechanisms in direct and inverse emulsions", *Journal of Rheology*, 62, 1495-1513 (2018)
- [51] Rabideau B.D., P. Moucheron, F. Bertrand, S. Rodts, Y. Meline, C. Lanos, P. Coussot, "Internal flow characteristics of a plastic kaolin suspension during extrusion", *J. Am. Ceram. Soc.*, 95, 494-501 (2012)
- [52] N'gouamba E., J. Goyon, P. Coussot, "Elastoplastic behavior of yield stress fluids", *Phys. Rev. Fluids*, 4, 123301 (2019)